Transient Response in Cross-Ply Laminated Cylinders and Its Application to Reconstruction of Elastic Constants

X. Han[1,2,3]**, G. R. Liu**[1,2] **and G. Y. Li** [1]

Abstract: An efficient hybrid numerical method is presented for investigating transient response of cross-ply laminated axisymmetric cylinders subjected to an impact load. In this hybrid numerical method, the laminated cylinder is divided into layered cylindrical elements in the thickness direction. The Hamilton principle is used to develop governing equations of the structure. The displacement response is determined by employing the Fourier transformations and the modal analysis. Numerical examples for analyzing transient waves have been provided in axisymmetric laminated cylindrical structures, both for thin cylindrical shells and thick cylinders.

A computational inverse technique is also presented for reconstructing elastic constants of axisymmetric cross-ply laminated cylinders from the surface displacement response data, using the present hybrid numerical method as the forward solver and neural network as the inverse operator. This technique is utilized to reconstruct the elastic constants of an axisymmetric laminated cylindrical shell.

keyword: Composite laminate, circular cylindrical structure, axisymmetric, material characterization, elastic wave, NDT, neural network.

1 Introduction

Composite cylindrical structures have high strength and stiffness, low coefficient of thermal expansion and excellent corrosion resistance. Besides, they also possess an ease of fabrication, a relative low-cost process and well-adapted production. In the application of laminated cylindrical structures to aerospace, nuclear and automo-bile industries, analyses of transient waves in them are of very importance. Furthermore, the property evaluation of laminated cylindrical shells has been one of the focuses of research.

There have been considerable works on wave propagation problems related to composite cylindrical shells. Chou and Achenbach (1981) provided a three-dimensional solution for orthotropic shells. Yuan et al. (1988) proposed an analytical method for the investigation of free harmonic wave propagation in laminated shells. Li et al. (1994) investigated the transient response of a cylindrical shell of finite length to transverse impact. Markus and Mead (1995a, b) presented an analytical method for investigating the dispersion behavior of waves in orthotropic laminated cylindrical shells. Because of the absence of a simple general solution for the shell waves, there are some numerical-analytical methods are proposed for waves propagating in composite shells. Nelson et al. (1971) proposed a numerical-analytical method (NAM) for analyzing waves in laminated orthotropic cylinders. In the analysis, the circumferential and axial displacements are represented by trigonometric functions, while the radial displacement is modeled by finite elements. Rattanwangcharoen et al. (1994, 1997) attacked the reflection problem of waves at the free edge of laminated circular cylinders. Zhuang et al. (1999) gave the construction of elastodynamic Green's function for laminated anisotropic cylinders. Xi et al. (2000) examined waves scattered by a crack in fluid-loaded axisymmetric laminated composite cylinders. Han et al. dealt with transient responses (2001) of cylindrical shells made of functionally gradient materials, and characteristics of waves (Han et al., 2002) in a functionally graded cylindrical shell. Verbis et al. (2002) investigated the elastic wave propagation in fiber reinforced composite materials with non-uniform distribution of fibers.

Advanced nondestructive methods for material charac-

[1] College of Mechanical and Automotive Engineering, Hunan University, Changsha 410082 Hunan, P.R. China
[2] Centre for Advanced Computations in Engineering Science (ACES) Department of Mechanical Engineering, National University of Singapore 10 Kent Ridge Crescent, Singapore 119260
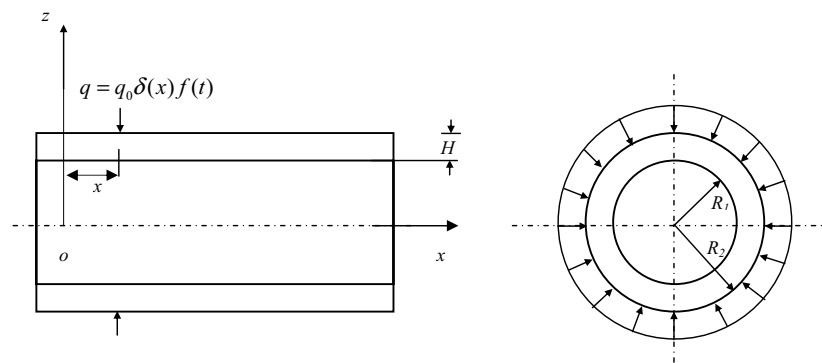[3] Tel/Fax: 65-68744795; Email:acehanxu@nus.edu.sg

Figure 1 : A laminated circular cylindrical shell constituted with cross-ply layers.

terization of composite utilize complex relationships between the structure behaviors and material property. These relationships are often represented by a known mathematical model, which defines the forward problem. Thus if a set of reasonably accurate experimentally measured structure behaviors data is available, material property of composite may be identified by solving an inverse problem properly formulated. In an inverse process, the efficiency of the forward solver is the important factor affecting the performance, as it is usually called many times in the inverse process.

Considerable works have been done in the inverse identification of the properties of composite materials ((Mignogna, 1990; Mignogna et al., 1991; Chu and Rokhlin, 1994; Rokhlin and Wang, 1992; Chao et al., 2001; Skovoroda and Goldstein, 2003; Sheen et al., 2003). Neural network (NN) techniques have also been applied in solving inverse problems. Examples include the reconstruction of constitutive properties using depth-load responses (Huber and Tsakmak, 1999) and using group velocities, phase velocities or slowness measurements (Sribar, 1994). Recently, a progressive NN approach (Liu et al., 2001) is suggested to characterize the material property of functionally graded material plate using the elastic waves. NN approaches can offer the advantages of very high efficient inversion operation and can avoid the need for thousands of times of calling of forward solvers. The hybrid numerical method (HNM) (Liu et al., 1991; Liu and Xi, 2001) is one of the most efficient numerical tools for 2D or 3D transient wave analysis in composite laminated plates. The efficiency is achieved by combining the finite element technique with the numerical Fourier transformation technique as well as the model analysis technique for dealing with the

time integration. This paper consists two important parts. The first part is to apply the process of HNM for calculating the transient response of laminated cylinders. In this method, the laminated cylinder is divided into layered cylindrical elements in the thickness direction. The Hamilton principle is used to develop governing equations of the cylinder. The displacement response is determined by employing the Fourier transformations and the modal analysis. This hybrid numerical method can reduce the number of elements, thus it has outstanding computation efficiency in the transient wave analysis of laminated cylindrical shells and paves the way for inverse operations. The other part is to suggest a computational inverse technique for reconstructing elastic constants of laminated cylinder using the present hybrid numerical method and the NN model. Numerical examples are presented to demonstrate the efficiency of the presented forward solver and the computational inverse technique.

2 Hybrid numerical method

Consider a laminated composite circular cylindrical shell made of an arbitrary number of linearly elastic shell-like plies. The thickness, inner radius and outer radius of the cylinder are denoted by H, R_1, R_2 respectively, as shown in Figure 1. Let x and z denote respectively the axial and radial coordinates. The cylinder is subjected to a radial line load of $q = q_0\delta(x)f(t)$ uniformly distributed along the circumferential direction, where δ is the Dirac delta function, and $f(t)$ is a function of the time. Because the geometry of the cylinder and the load are independent of the circumferential direction, the problem is axisymmetric.
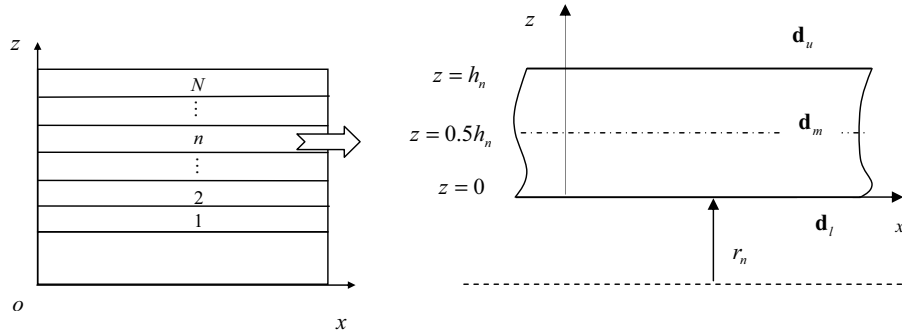
Figure 2 : Annular element subdivision and the *n*th isolated annular element.

The stain-displacement relations are given by

$$\varepsilon = \mathbf{L}\mathbf{U} \tag{1}$$

where $\varepsilon = \begin{bmatrix} \varepsilon_x & \varepsilon_\theta & \varepsilon_z & \varepsilon_{xz} \end{bmatrix}^T$ is the vector of stains, $\mathbf{U} = [u \ w]^T$ is the vector of displacements, u and w are the displacements in the axial and radial directions, respectively, and $\mathbf{L}$ is the operator matrix

$$
\mathbf{L} = \mathbf{L}_1 \frac{\partial}{\partial x} + \mathbf{L}_2 \frac{\partial}{\partial z} + \mathbf{L}_3 \frac{1}{R_1 + z}
$$

$$
= \begin{bmatrix} 1 & 0 \\ 0 & 0 \\ 0 & 0 \\ 0 & 1 \end{bmatrix} \frac{\partial}{\partial x} + \begin{bmatrix} 0 & 0 \\ 0 & 0 \\ 0 & 1 \\ 1 & 0 \end{bmatrix} \frac{\partial}{\partial z}
$$

$$
+ \begin{bmatrix} 0 & 0 \\ 0 & 1 \\ 0 & 0 \\ 0 & 0 \end{bmatrix} \frac{1}{R_1 + z} \tag{2}
$$

where the radial coordinate is decomposed as $R_1 + z$. The stresses are related to strains by

$$\sigma = \mathbf{c}\varepsilon \tag{3}$$

where $\sigma = \begin{bmatrix} \sigma_x & \sigma_\theta & \sigma_z & \sigma_{xz} \end{bmatrix}^T$ is the vector of stresses and $\mathbf{c}$ is the matrix of the elastic constants of the lamina,

$$
c = \begin{bmatrix} c_{11} & c_{12} & c_{13} & 0 \\ c_{12} & c_{22} & c_{23} & 0 \\ c_{13} & c_{23} & c_{33} & 0 \\ 0 & 0 & 0 & c_{55} \end{bmatrix} \tag{4}
$$

whose expressions in terms of engineering constants are given in detail by Vinson and Sierakowski (1987).

We proceed with the derivation of the HNM formula. The annular elements are used to model the radial displacement component of the shell, while the axial and circumferential displacement components are dealt with analytically. In view of the heterogeneity of the laminated cylindrical shell in the radial direction, an annular element shown in Figure 2 is used in the subdivision of the shell so as to achieve high computational precision. The thickness and inner radius of the *n*th element are denoted by h_n and r_n, respectively. It can be found that the outer radius of the *n*th element is equal to $r_n + h_n$. The elastic constants in each annular element are the same.

Approximating the displacement field within an element as

$$\mathbf{U} = \mathbf{N}\mathbf{d} \tag{5}$$

where $\mathbf{N}$ is the shape function matrix of second order given by

$$\mathbf{N} = [(1 - 3\bar{z} + 2\bar{z}^2)\mathbf{E} \ \ 4(\bar{z} - \bar{z}^2)\mathbf{E} \ \ (2\bar{z}^2 - \bar{z})\mathbf{E}] \tag{6}$$

Here $\mathbf{E}$ is a 2 by 2 identity matrix and $\bar{z} = z/h_n$, and $\mathbf{d}$ is the displacement amplitude vector at $z = 0$, $z = 0.5h_n$ and $z = h_n$ as follows:

$$\mathbf{d} = [d_l^T \ d_m^T \ d_u^T]^T \tag{7}$$

Taking variation with respect to $\mathbf{U}$ following the Hamilton principle, leads to the following governing ordinary differential equations of the element (Liu et al., 1991):

$$\mathbf{q} = \mathbf{M}\ddot{\mathbf{d}} + \mathbf{K}_D \mathbf{d} \tag{8}$$

where the dot represents the derivative with respect to the time, and

$$\mathbf{K}_D = -\mathbf{A_2}\frac{d^2}{dx^2} + \mathbf{A_1}\frac{d}{dx} + \mathbf{A_0} \tag{9}$$

The subscript 'D' denotes that **K** is a differential operator matrix. Matrices **M** and **q** are the mass matrix and the load matrix, respectively. The expressions for matrices $\mathbf{A}_i (i = 0, 1, 2)$ and **M** are given in the appendix.

As it can be seen from equation (9), the original partial differential equations of the cylinder with three variables (x, z, t) have simplified to a system of ordinary differential equations by the above procedure. Assembling all the elements, a system of approximate differential equations for the whole cylinder may be expressed as

$$\mathbf{q}_t = \mathbf{M}_t \ddot{\mathbf{d}}_t + \mathbf{K}_{D_t} \mathbf{d}_t \tag{10}$$

where

$$\mathbf{K}_{Dt} = -\mathbf{A_2}_t \frac{d^2}{dx^2} + \mathbf{A_1}_t \frac{d}{dx} + \mathbf{A}_{0t} \tag{11}$$

In these equations, the subscript 't' denotes matrices or vectors for the whole cylinder. The matrices $\mathbf{A}_{it} (i = 0, 1, 2)$, $\mathbf{M}_t$ and the vectors $\mathbf{q}_t, \mathbf{d}_t$ can be obtained by assembling the corresponding matrices and vectors of adjacent elements. The sizes of $\mathbf{d_t}$ and $\mathbf{q_t}$ are $M \times 1$, and the sizes of the matrices $\mathbf{M}_t$ and $\mathbf{A}_{it}$ are $M \times M$, where $M = 2 \times (2N + 1)$ and N is the number of the layer element.

The application of the Fourier transformations to equation (11) leads to

$$\tilde{\mathbf{q}}_t = \mathbf{M}_t \ddot{\tilde{\mathbf{d}}}_t + \mathbf{K}_t \tilde{\mathbf{d}}_t \tag{12}$$

where $\tilde{\mathbf{d}}$ and $\tilde{\mathbf{q}_t}$ are the Fourier transformations of $\tilde{\mathbf{d}}$ and $\mathbf{q_t}$, respectively, and $\mathbf{K}_t$ is the stiffness matrix given by

$$\mathbf{K}_t = k^2 \mathbf{A}_{2t} + ik\mathbf{A}_{1t} + \mathbf{A}_{0t} \tag{13}$$

where k is the wavenumber of the axial direction.

The modal analysis is used to obtain the Fourier transformation of the displacement vector. Solving the following eigenvalue equation corresponding to equation (12),

$$0 = [\mathbf{K}_t - \omega^2 \mathbf{M}_t]\phi^R \tag{14}$$

The eigen-frequencies $\omega_m (m = 1, 2, 3...M)$ and the corresponding right eigenvectors ϕ_m^R can be obtained. For a time-step impact load, the displacement in the Fourier transformation domain is given following the method given by (Liu et al., 1991; Liu and Xi, 2001):

$$\tilde{\mathbf{d}}_t^{(}k,t) = \sum_{m=1}^{M} \frac{\phi_\mathbf{m}^\mathbf{L} \tilde{\mathbf{q}}_t \phi_\mathbf{m}^\mathbf{R} (1 - \cos \omega_m t)}{\omega_m^2 M_m} \tag{15}$$

where $\omega_m, \phi_\mathbf{m}^\mathbf{R}$ and $\phi_\mathbf{m}^\mathbf{L}$ are the mth eigenfrequency and the corresponding right and left eigenvectors, and

$$M_m = \phi_\mathbf{m}^L \mathbf{M}_t \phi_\mathbf{m}^\mathbf{R} \tag{16}$$

Taking the inverse Fourier transformation, the displacement response in the space-time domain can be expressed by

$$\mathbf{d}_t^{(}x,t) = \frac{1}{2\pi} \int_{-\infty}^{+\infty} \tilde{\mathbf{d}}_t(k,t) e^{-ikx} dk \tag{17}$$

The integration in equation (17) can be carried out by using the fast Fourier transform (FFT) techniques.

It should be noted that the present treatment solves the governing equation as an eigenvalue problem at each wavenumber with real eigenvalues, numerically integrate over wavenumbers to get the solution in frequency domain. In this treatment, we cannot get the close solution in frequency domain. The major aspect of this treatment is that the solution in time domain can be obtained without any singularities over the integration path. Based on our experience in numerical performance, this treatment is more efficient for numerical calculation for transient response in time domain. Furthermore, several numerical techniques (Liu et al., 1997; Liu and Lam, 1996) have been suggested to further improve the efficiency of the present treatment in calculating the displacement response in time domain.

The present HNM is different to other treatment as that solves the governing equation as an eigenvalue problem at each given frequency, then integrated analytically over the wavenumbers to get the solution in frequency domain. The frequency solution can be analytically obtained, and this treatment is considered as a more efficient method for analysis of waves in the frequency domain. However, in the numerical performance of this treatment, the eigenvalues are generally complex values, and the numerical integration over frequencies to the time domain needs to avoid the singularities over the integral path. For examples of this kind treatment, the authors are suggested to refer (Zhuang et al., 1999; Liu and Lam, 1996).

3   Numerical results and discussions

In this section, numerical results are presented for transient response of impact loads in laminated composite

cylinder. In laminate codes used below, a lamina numbering increases from the inner to outer surface; letters *C* and *G* represent carbon/epoxy and glass/epoxy, respectively; the number following the letters indicates the azimuthal angle of the fiber orientation with respect to the *x* axis; the subscript *s* denotes that the multilayered shell is symmetrically stacked about the middle surface. The material constants of carbon/epoxy and glass/epoxy are provided by Takahashi and Chou (1987).

In the calculations, the follows dimensionless parameters are used:

$$\bar{x} = x/H, \quad \bar{c}_{ij} = c_{ij}/c_{55}^c, \quad \bar{w} = c_{55}^c w/q_0 R_2,$$
$$\bar{u} = c_{55}^c u/q_0 R_2, \quad \bar{\omega} = \omega h/c_s$$
$$c_s = \sqrt{c_{55}^c/\rho_c}, \quad \bar{r} = r/H, \quad \bar{\rho} = \rho/\rho_c \quad (18)$$

where c_{55}^c and ρ_c stand for the reference material constant and mass density. Here they are equal to the material constant c_{55} and mass density of the carbon/epoxy. Two ratios of the inner radius to thickness, $R_1 = H$ and $R_1 = 20H$ are employed in the following calculations, the former is viewed as a thick circular cylinder, and the latter is viewed as a thin circular cylindrical shell.

The time history of the incident wavelet is given as

$$f(t) = \begin{cases} \sin(2\pi t/t_d) & 0 < t < t_d \\ 0 & t \leq 0 \text{ and } t \geq t_d \end{cases} \quad (19)$$

where t_d is the time duration of the incident wavelet and $\omega_f = \frac{2\pi}{t_d}$. In this paper, we set $\bar{t}_d = 2.0$. It means that the wavelet is one cycle of the sine function.

Figures 3 (a) and 3(b) show the time history of the displacements in the axial and radial direction on the outer surface of a glass-carbon [C90/G0/G90]$_s$ cylindrical shell ($R_1 = 20H$) subjected to a radial line load defined by equation (19) uniformly distributed along the circumferential direction at $x = 0$, respectively. In the simulation, each ply is divided into 4 layers. A comparison of the displacement response between glass [G90/G0]$_s$ and carbon [C90/C0]$_s$ laminated cylindrical shells is also presented in this figure. It can be observed from Figure 3(b) that the peak value of displacement response in the radial direction for the carbon-glass cylindrical shell is less than that for the carbon cylindrical shell also the glass one. Figures 4(a) and 4(b) show the time history of the displacements in the axial and radial
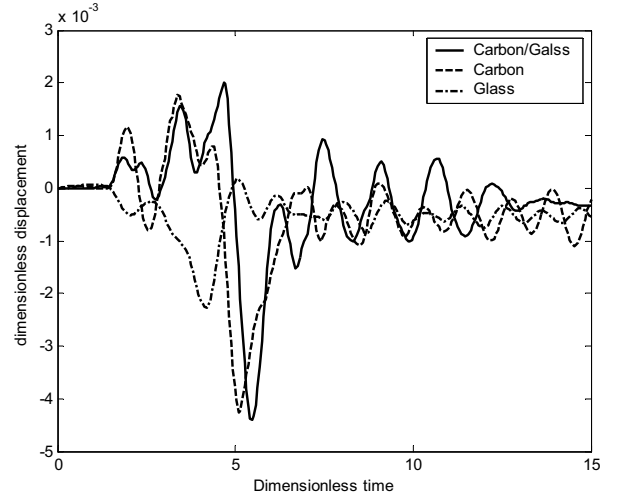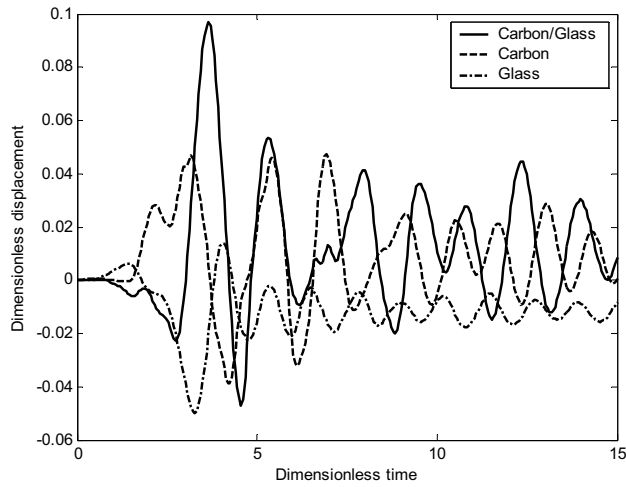
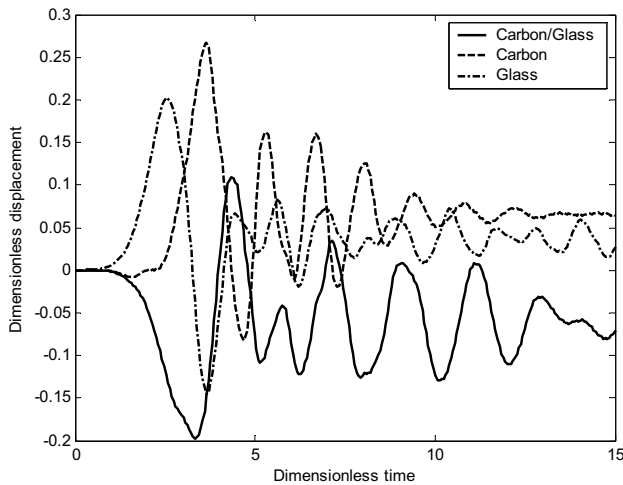

(a) Displacement in axial direction
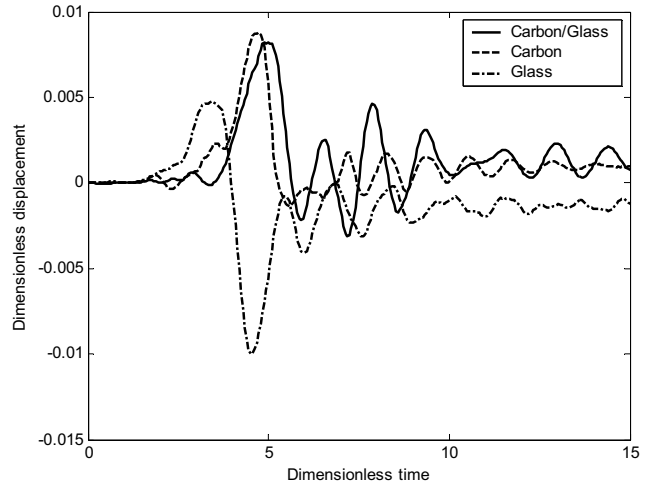
(b) Displacement in radial direction

Figure 3 : The time history of the displacement at $\bar{x} = 5$ on the outer surface of cylindrical shells ($R_1 = 20H$) subjected to a radial line load defined by equation (23) uniformly distributed along the circumferential direction at $x = 0$

direction, but for the glass-carbon [C90/G0/G90]$_s$ cylinder ($R_1 = H$). The comparison of the displacement response between glass [G90/G0]$_s$, and carbon [C90/C0]$_s$ laminated cylinder is also presented. Same property but more clear as Figure 3(b) can be observed from Figurer 4(b) that the peak value of displacement response in the radial for the carbon-glass cylinder is less than that for the carbon cylindrical shell also the glass one, From these

(a) Displacement in axial direction

(b) Displacement in radial direction

Figure 4 : Same as Figure 3 but for the cylinder ($R_1 = 2H$)

Figure 5 : Displacement in axial direction on the outer surface in the $z-t$ plane of the $[G0/90]_s$ cylindrical shell ($R_1H = 20$)

Figure 6 : Same as Figure 5 but for displacement in radial direction

results, it can be conclude that the carbon-glass laminated cylindrical shell have better properties for attenuation of the displacement response in the radial direction induced by the same source of excitation.

To show the characteristics of waves, the so-called $x-t$ plane (Graff, 1991) is often used. Due to the aniosortropy of the shells, and the presence of boundaries, all kinds of waves are dispersive vector waves, and coupled to each other. Therefore there is no pure longitudinal wave (P wave), or shear wave (S wave). Also, it is impossible to observe clear wave fronts of these waves in the $x-t$
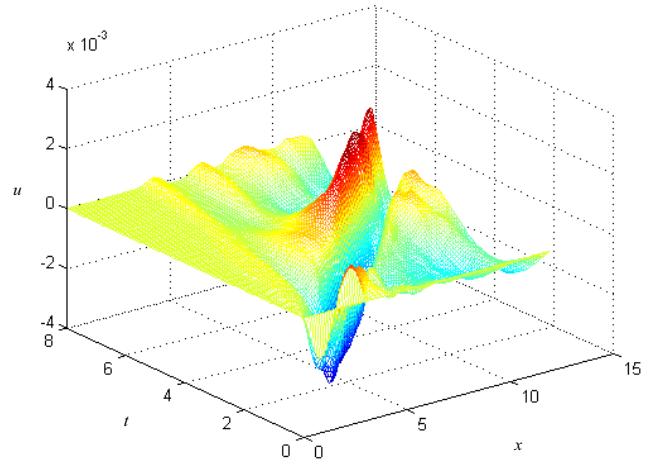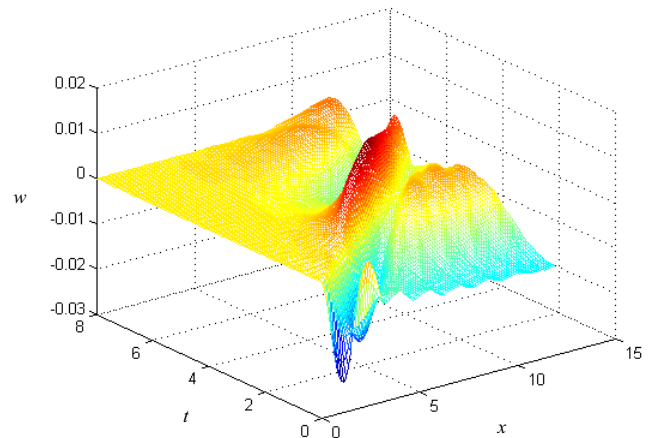
plane. However, waves having similar properties of P and S waves can be still observed in the $x-t$ plane. Figures 5 and 6 show the $x-t$ plane for the displacement response u and w on the upper surface of the $[G0/90]_s$ shells subjected to a radial line load defined by equation (19) uniformly distributed along the circumferential direction at $x = 0$, respectively. From these two figures, it can be seen that at different times, different forms of wave field are observed. The form of the wave field is changing while waves are propagating, because the waves are scattered by the boundaries and anisotropy of the shell. From Figure 5 the wave front of the pseudo-P wave can

be quite clearly observed, as the displacement response u is sensitive to the pseudo-P wave. The wave front for the pseudo-P wave is less obvious in Figure 6, due to the displacement response w is less sensitive than the displacement response u. The wave front for the pseudo-S wave is quite obvious.

A Fortran 90 program developed using proposed method only needs about 25 second in a SGI Origin 2000 computer to calculate a 4-layer laminated axisymmetric shell. This method has outstanding computation efficiency for the wave analysis of laminated cylinders, thus it is used for the following inverse procedure.

4 Applications to reconstruction of material constants

4.1 Statement of the problem

Consider an axisymmetric cross-ply laminated cylindrical shell ($R_1 = 20H$) with any number of anisotropic layers in the thickness direction. The incident excitation waves to the laminated cylindrical shell are assumed to be a radial line load acting at $x = 0$ on the upper surface. The line load is defined by equation (19). Only one receiving point is chosen on the outer surface of the laminated cylindrical shell. An NN model is used for the determination of elastic constants of anisotropic laminated shells. The outputs of the NN model are elastic constants. The displacement components in x directions are selected as the inputs for the NN model.

In this paper, the progressive NN procedure (Liu et al., 2001; Liu and Han, 2003) is employed as the inverse technique to reconstructing the elastic constants of laminated cylindrical shell. The proposed hybrid numerical method is employed as the teacher of the NN model. A brief description of the principle of the progressive NN procedure is given as follows.

An NN model is trained using initial training data containing a set of assumed elastic constants, which represents various elastic constants of laminated cylindrical shell, and their corresponding displacement responses calculated from the HNM. A neural network requires a large training set to successfully learn and to generalize the characteristic features from input-output pairs. Consequently, it is essential that the calculation of the forward problem is performed as efficiently as possible to generate the training data set. The HNM is employed as the teacher for training the NN model.

After the initial training of the NN model, the determination of the elastic constants begins by feeding the measured displacement response data $\mathbf{X}_m$ into the NN model. The outputs of the NN model are the determined elastic constants $\mathbf{Y}_I$. These determined elastic constants are then fed into the HNM to produce a set of calculated displacement response data $\mathbf{X}_c$. A comparison between the calculated displacement response $\mathbf{X}_c$ and measured displacement responses $\mathbf{X}_m$ is made based on a given criterion. If these two sets differ significantly such that the criterion is not satisfied, then the NN model will be retrained on-line using adjusted training samples that contain $\mathbf{X}_c$ and $\mathbf{Y}_I$. The retrained NN model is then used to determine the elastic constants again by feeding in the measured displacement responses $\mathbf{X}_m$. This determination and on-line retraining procedure is repeated until the difference between the calculated and measured displacement responses satisfies the given criterion. At the end of the progression, the final determined elastic constants are guaranteed to produce the displacement responses that are very close to the measured ones when fed into the hybrid numerical method.

4.2 Reconstruction Examples

Consider a simple case that the laminated cylindrical shell is assumed to be made by the same material, but with different ply-angles 0^0 or 90^0 for different layers. We somehow know the ply-angles of each layers, we want to determine the on-principal-axis elastic constants from the displacement response.

Table 1 : The search range for the elastic constants for glass/epoxy laminated cylindrical shell

Elastic Constants	Actual Data (GPa)	Search Range (GPa)
c_{11}	42.020	30-54
c_{12}	6.067	4-8
c_{22}	13.500	10-18
c_{23}	7.277	5-9
c_{55}	3.410	2-4

Elastic constants of the glass/epoxy [G90/0]$_s$ laminated cylindrical shell are determined. The glass/epoxy mate-

Table 2 : Reconstructed results of elastic constants of glass/epoxy [0/90] $_s$ laminated cylindrical shell

Elastic Constants	Original Value (GPa)	Result (deviation) at progressions			
		1	2	3	4
(a) noise free					
c_{11}	42.020	41.644(0.9%)	42.936(2.2%)	42.924(2.2%)	42.631(1.5%)
c_{12}	6.067	6.698(10.4%)	6.658(9.7%)	6.576(8.4%)	6.456(6.4%)
c_{22}	13.500	14.240(5.4%)	14.123(4.6%)	13.385(0.9%)	13.798(2.2%)
c_{23}	7.277	7.868(7.7%)	7.861(8.0%)	7.657(5.2%)	7.469(2.6%)
c_{55}	3.410	3.491(2.4%)	3.543(3.9%)	3.609(5.8%)	3.517(3.1%)
(b) noise-added					
c_{11}	42.020	43.544(3.6%)	42.620(1.4%)	42.622(1.4%)	42.530(1.2%)
c_{12}	6.067	6.998(15.3%)	6.607(8.9%)	6.594(8.7%)	6.402(5.5%)
c_{22}	13.500	13.876(2.8%)	14.022(3.9%)	13.322(1.3%)	13.873(2.8%)
c_{23}	7.277	7.987(9.8%)	8.026(10.3%)	7.61(4.6%)	7.765(6.7%)
c_{55}	3.410	3.392(-0.5%)	3.512(3.0%)	3.562(4.5%)	3.575(4.8%)

rial is the transversely isotropic material; there are only five on-principal-axis elastic constants as listed in the 2nd column in Table 1. Hence there are five parameters, named as $c_{11}, c_{12}, c_{22}, c_{23}$ and c_{55} need to be determined. The search range for the five parameters is set between –30% and +30% off from the actual values as shown in Table 1. Both the noise free and noise-contaminated displacement response is used for the reconstruction of the elastic constants. The Gauss noise is directly added to the computer-generated displacements. A vector of pseudo-random number is generated from a Gauss distribution with mean a and standard deviation b. The mean a is set to zero, and the standard deviation b is $0.01 \times [1/n_s \sum_{i=1}^{n_s} (u_i^m)^2]^{0.5}$, where u_i^m is the computer-generated displacement reading at the ith sample point, n_s is the number of sample.

Table 2 summarizes the reconstructed results of the elastic constants. The results for four progressions are listed. It can be found that the result at the first progression is not accurate as the maximum deviation is high, and the displacement responses corresponding to these reconstructed elastic constants are quite different from the simulated ones using the actual values of elastic constants. A retraining for NN model is required. A new sample is created from the 1st determined result and the corresponding displacement responses calculated from the hybrid numerical method. The new sample is added into the original sample pool to replace the sample with large

distance norm (Liu et al., 2001). The retraining process is repeated until the displacement responses corresponding to the reconstructed elastic constants are sufficiently close to the simulated measurements. The results at stages of progressive training are also listed in Table 2. It can be seen from Table 2 that the accuracy of the determined results increase as the progression number increases, and the determined result is very accurate after 4 progressions. The maximum deviation of the sixth progression elastic constants is as low as 6%. It can be also found that, the determined result remains stable regardless the presence of the noise, and the required number of progression is not changed, even when the noise is added.

This section mainly addressed the computational method of the material constant reconstruction using elastic waves and neural networks. The practical application of the presented NN procedure relies on the tests of real structures, and the NN procedure should be validated using practical experimental results. However, it should be noted that it is often very difficult to train an NN model for complex relationship between material property and the dynamic responses to be valid in a wide range of parameters and for more parameters.

5   Conclusions

In this paper, a HNM is presented for analyzing the transient response of cross-ply axisymmetric laminated shells excited by a radial line impact load. In this method,

the laminated cylindrical shell is divided into layered cylindrical elements in the thickness direction. The Hamilton principle is used to develop governing equations of the laminated cylindrical shell. The displacement response is determined by employing the Fourier transformations and the modal analysis. The solution in time domain can be obtained without any singularities over the integration path. This method has outstanding computation efficiency in the transient wave analysis of laminated cylindrical shells and paves the way for inverse operations.

A computational inverse technique is presented for reconstruction of elastic constants of laminated cylindrical shells using the hybrid numerical method. It can be found that this computational inverse technique could provide an accurate prediction of the elastic constants of laminated cylindrical shells from the displacement response data measured on the surface. The present HNM can be used as a forward solver in an inverse process for material constant reconstruction of axisymmetric laminated cylindrical shells.

Appendix

$$\mathbf{A}_0$$
$$= \frac{1}{6h_n}$$
$$\begin{bmatrix} (14r_n+3h_n)\mathbf{D}_3 & -(16r_n+4h_n)\mathbf{D}_3 & (2r_n+h_n)\mathbf{D}_3 \\ -(16r_n+4h_n)\mathbf{D}_3 & (32r_n+16h)_n\mathbf{D}_3 & -(16r_n+12h_n)\mathbf{D}_3 \\ (2r_n+h_n)\mathbf{D}_3 & -(16r_n+12h_n)\mathbf{D}_3 & (14r_n+11h_n)\mathbf{D}_3 \end{bmatrix}$$
$$+\frac{1}{3}\begin{bmatrix} -3\mathbf{D}_5 & 4\mathbf{D}_5 & -\mathbf{D}_5 \\ -4\mathbf{D}_5 & 0 & 4\mathbf{D}_5 \\ \mathbf{D}_5 & -4\mathbf{D}_5 & 3\mathbf{D}_5 \end{bmatrix}$$
$$+\frac{1}{6h_n^4}\begin{bmatrix} \alpha_{11}\mathbf{D}_6 & \alpha_{12}\mathbf{D}_6 & \alpha_{13}\mathbf{D}_6 \\ \alpha_{12}\mathbf{D}_6 & \alpha_{22}\mathbf{D}_6 & \alpha_{23}\mathbf{D}_6 \\ \alpha_{13}\mathbf{D}_6 & \alpha_{23}\mathbf{D}_6 & \alpha_{33}\mathbf{D}_6 \end{bmatrix}$$

$$\mathbf{D}_3 = \mathbf{L}_2^T \mathbf{c}\mathbf{L}_2 = \begin{bmatrix} 0 & 0 \\ 0 & c_{33} \end{bmatrix}$$

$$\mathbf{D}_5 = \frac{1}{2}(\mathbf{L}_2^T \mathbf{c}\mathbf{L}_3 + \mathbf{L}_3^T \mathbf{c}\mathbf{L}_2) = \begin{bmatrix} 0 & 0 \\ 0 & c_{23} \end{bmatrix}$$

$$\mathbf{D}_6 = \mathbf{L}_3^T \mathbf{c}\mathbf{L}_3 = \begin{bmatrix} 0 & 0 \\ 0 & c_{22} \end{bmatrix}$$

$$\alpha_{11} = -24h_n r_n^3 - 15h_n^4 - 60h_n^2 r_n^2 - 50h_n^3 r_n$$
$$+ 6\ln(r_n+h_n)h_n^4 + 36\ln(r_n+h_n)r_n h_n^3$$
$$+ 78\ln(r_n+h_n)R_n^2 h_n^2 + 72\ln(r_n+h_n)R_n^3 h_n$$
$$+ 24\ln(r_n+h_n)r_n^4 - 6\ln(r_n)h_n^4$$
$$- 36\ln(r_n)r_n h_n^3 - 78\ln(r_n)r_n^2 h_n^2 - 72\ln(r_n)r_n^3 h_n$$
$$- 24\ln(r_n)r_n^4$$

$$\alpha_{12} = -4\left[-12h_n r_n^3 - h_n^4 - 24h_n^2 r_n^2 - 13h_n^3 r_n\right.$$
$$+ 6\ln(r_n+h_n)r_n h_n^3 + 24\ln(r_n+h_n)r_n^2 h_n^2$$
$$+ 30\ln(r_n+h_n)r_n^3 h_n + 12\ln(r_n+h_n)r_n^4$$
$$- 6\ln(r_n)r_n h_n^3 - 24\ln(r_n)r_n^2 h_n^2$$
$$\left.- 30\ln(r_n)r_n^3 h_n - 12\ln(r_n)r_n^4\right]$$

$$\alpha_{13} = -24h_n r_n^3 - h_n^4 - 36h_n^2 r_n^2 - 14h_n^3 r_n$$
$$+ 6\ln(r_n+h_n)r_n h_n^3 + 30\ln(r_n+h_n)r_n^2 h_n^2$$
$$+ 48\ln(r_n+h_n)r_n^3 h_n + 24\ln(r_n+h_n)r_n^4$$
$$- 6\ln(r_n)r h_n^3 - 30\ln(r_n)r_n^2 h_n^2$$
$$- 48\ln(r_n)r_n^3 h_n - 24\ln(r_n)r_n^4$$

$$\alpha_{22} = 8\left[-12h_n r_n^3 + h_n^4 - 18h_n^2 r_n^2 + 12\ln(r_n+h_n)r_n^2 h_n^2\right.$$
$$- 4h_n^3 r_n + 24\ln(r_n+h_n)r_n^3 h_n + 12\ln(r_n+h_n)r_n^4$$
$$\left.- 12\ln(r_n)r_n^2 h_n^2 - 24\ln(r_n)r_n^3 h_n - 12\ln(r_n)r_n^4\right]$$

$$\alpha_{23} = -4\left[-12h_n r_n^2 - 12h_n^2 r_n + 6\ln(r_n+h_n)r_n h_n^2 - h_n^3\right.$$
$$+ 18\ln(r_n+h_n)r_n^2 h_n + 12\ln(r_n+h_n)r_n^3 - 6\ln(r_n)r_n h_n^2$$
$$\left.- 18\ln(r_n)r_n^2 h_n - 12\ln(r_n)r_n^3\right]$$

$$\alpha_{33} = -24h_n r_n^3 + h_n^4 - 12h_n^2 R_n^2 + 6\ln(r_n+h_n)r_n^2 h_n^2$$
$$- 2h_n^3 r_n + 24\ln(r_n+h_n)r_n^3 h_n + 24\ln(r_n+h_n)r_n^4$$
$$- 6\ln(r_n)r_n^2 h_n^2 - 24\ln(r_n)r_n^3 h_n - 24\ln(r_n)r_n^4$$

$\mathbf{A}_1$

$= \dfrac{1}{15}$

$$\begin{bmatrix} -(15r_n+2h_n)\mathbf{D}_2 & -(20r_n+6h_n)\mathbf{D}_2 & (5r_n+3h_n)\mathbf{D}_2 \\ (20r_n+4h_n)\mathbf{D}_2 & -8h_n\mathbf{D}_2 & -(20r_n+16h_n)_n\mathbf{D}_2 \\ -(5r_n+2h_n)\mathbf{D}_2 & (20r_n+14h_n)\mathbf{D}_2 & (15r_n+13h_n)\mathbf{D}_2 \end{bmatrix}$$

$$-\dfrac{1}{30}\begin{bmatrix} -(30r_n+4h_n)\mathbf{D}'_2 & -2h_n\mathbf{D}'_2 & h_n\mathbf{D}'_2 \\ -2h_n\mathbf{D}'_2 & -16h_n\mathbf{D}'_2 & -2h_n\mathbf{D}'_2 \\ h_n\mathbf{D}'_2 & -2h_n\mathbf{D}'_2 & (30r_n+26h_n)\mathbf{D}'_2 \end{bmatrix}$$

$$+\dfrac{h_n}{15}\begin{bmatrix} 4\left(\mathbf{D}_4-\mathbf{D}'_4\right) & 2\left(\mathbf{D}_4-\mathbf{D}'_4\right) & -\left(\mathbf{D}_4-\mathbf{D}'_4\right) \\ 2\left(\mathbf{D}_4-\mathbf{D}'_4\right) & 16\left(\mathbf{D}_4-\mathbf{D}'_4\right) & 2\left(\mathbf{D}_4-\mathbf{D}'_4\right) \\ -\left(\mathbf{D}_4-\mathbf{D}'_4\right) & 2\left(\mathbf{D}_4-\mathbf{D}'_4\right) & 4\left(\mathbf{D}_4-\mathbf{D}'_4\right) \end{bmatrix}$$

$$\mathbf{D}_2 = \dfrac{1}{2}(\mathbf{L}_1^T\mathbf{c}\mathbf{L}_2+\mathbf{L}_2^T\mathbf{c}\mathbf{L}_1) = \dfrac{1}{2}\begin{bmatrix} 0 & c_{13} \\ c_{13} & 0 \end{bmatrix}$$

$$\mathbf{D}_4 = \dfrac{1}{2}(\mathbf{L}_1^T\mathbf{c}\mathbf{L}_3+\mathbf{L}_3^T\mathbf{c}\mathbf{L}_1) = \dfrac{1}{2}\begin{bmatrix} 0 & c_{12} \\ c_{12} & 0 \end{bmatrix}$$

$$\mathbf{D}'_4 = \mathbf{L}_1^T\mathbf{c}\mathbf{L}_3 = \begin{bmatrix} 0 & c_{12} \\ 0 & 0 \end{bmatrix}$$

$\mathbf{A}_2$

$$= \dfrac{h_n}{60}\begin{bmatrix} (8r_n+h_n)\mathbf{D}_1 & 4r_n\mathbf{D}_1 & -(2r_n+h_n)\mathbf{D}_1 \\ 4r_n\mathbf{D}_1 & (32r_n+16h_n)\mathbf{D}_1 & (4r_n+4h_n)\mathbf{D}_1 \\ -(2r_n+h_n)\mathbf{D}_1 & (4r_n+4h_n)\mathbf{D}_1 & (8r_n+7h_n)\mathbf{D}_1 \end{bmatrix}$$

$$\mathbf{D}_1 = \mathbf{L}_1^T\mathbf{c}\mathbf{L}_1 = \begin{bmatrix} c_{11} & 0 \\ 0 & c_{55} \end{bmatrix}$$

$$\mathbf{M} = \dfrac{\rho h_n}{60}\begin{bmatrix} (8r_n+h_n)\mathbf{E} & 4r_n\mathbf{E} & -(2r_n+h_n)\mathbf{E} \\ 4r_n\mathbf{E} & (32r_n+16h_n)\mathbf{E} & (4r_n+4h_n)\mathbf{E} \\ -(2r_n+h_n)\mathbf{E} & (4r_n+4h_n)\mathbf{E} & (8r_n+7h_n)\mathbf{E} \end{bmatrix}$$

$$\mathbf{q} = \begin{bmatrix} 0 & 0 & 0 & 0 & 0 & q_0R_2 \end{bmatrix}^T, \quad \mathbf{E} = \begin{bmatrix} 1 & 0 \\ 0 & 1 \end{bmatrix}$$

References

Chao, R. M.; Chen, Y. J.; Lin, F. C. (2001): Determining the unknown traction of a cracked elastic body using the inverse technique with the dual boundary element method, *CMES: Computer Modeling in Engineering & Sciences*, 2(1): 73-86.

Chou, F. H.; Achenbach, J. D. (1981): Three-dimensional vibrations of orthotropic cylinders, *ASCE Journal of Engineering Mechanics*. 98: 813-822.

Chu, Y. C.; Rokhlin, S. I. (1994): Stability of determination of composite moduli from velocity data in planes of symmetry for weak and strong anisotropies. *Journal of the acoustical society of America*, 95(1): 213-225.

Graff, K. F. (1991): *Wave motion in elastic solids, Dover Publications*, New York.

Han, X.; Liu, G. R.; Xi, Z. C.; Lam, K. Y. (2001): Transient waves in a functionally graded cylinder, *International Journal of Solids and Structures*, 38: 3021-3037

Han, X.; Liu, G. R.; Xi, Z. C.; Lam, K. Y. (2002): Characteristics of waves in a functionally graded cylinder, *International Journal for Numerical Methods in Engineering*, 53: 653-676.

Huber, N.; Tsakmakis, C. (1999): Determination of constitutive properties from spherical indentation data using neural networks, Part I: the case of pure kinematic hardening in plasticity laws, *Journal of the mechanics and physics solids*, 47: 1569-1588.

Li, S. M.; Hong, H. Z.; Ruiz, C. (1994): Transient response of a cylindrical shell of finite length to transverse impact. *International journal of solids and structures*. 27(4): 485-503.

Liu, G. R.; Han, X. (2003): *Computational inverse techniques in nondestructive evaluation*, CRC Press, Boca Raton.

Liu, G. R.; Han, X.; Lam, K. Y. (2001): Material characterization of functionally graded material using elastic waves and a progressive learning neural network, *Composite Science and Technology*, 61: 1401-1411.

Liu, G. R.; Tani, J.; Ohyoshi, T.; Watanabe, K. (1991): Transient waves in anisotropic laminated plates, Part 1: Theory; Part 2: Applications, *Journal of vibration and acoustics*. 113: 230-239.

Liu, G. R.; Xi, Z. C. (2001): *Elastic waves in anisotropic laminates*, CRC press, Boca Raton.

Liu, G. R.; Lam, K. Y.; Ohyoshi, T. (1997): A technique for analyzing elastodynamic responses of anisotropic laminated plates to line loads. *Composites Part B*. 28B: 667-677.

Liu, G. R.; Lam, K. Y. (1996): Two-dimensional time-harmonic elastodynamic Green's functions for anisotropic media". *International Journal of Engineering Sciences*, Vol. 34, 1996, pp. 1327-1338.

Markus, S.; Mead, D. J. (1995): Axisymmetric and asymmetric wave motion in orthotropic cylinders, *Jour-*

nal of Sound and Vibration, 181: 127-147.

Markus, S.; Mead, D. J. (1995): Wave motion in a 3-layered, orthotropic isotropic orthotropic composite shell, *Journal of Sound and Vibration*, 181: 149-167.

Mignogna, R. B. (1990): Ultrasonic determination of elastic constants from oblique angles of incidence in non-symmetry planes, *Review of progress in quantitative non-destructive evaluation*, edited by Thompson DO and Chimenti DE, Plenum Press. 9: 1565-1573.

Mignogna, R. B.; Batra, N. B.; Simmonds, K. E. (1991): Determination of elastic constants of anisotropic materials from oblique angle ultrasonic measurements. I: Analysis; II: Experimental, *Review of progress in quantitative nondestructive evaluation*, edited by Thompson DO and Chimenti DE Plenum Press, 10B: 1669-1684.

Nelson, R. B.; Dong, S. B.; Kalra, R. D. (1971): Vibrations and waves in laminated orthotropic circular cylinders, *Journal of Sound and Vibration*, 18: 429-444.

Rattanwangcharoen, N.; Shah, A. H.; Datta, S. K. (1994): Reflection of waves at the free edge of a laminated circular cylinder, *ASME Journal of Applied Mechanics* 61: 323-329.

Rattanwangcharoen, N.; Zhuang, W.; Shah, A. H.; Datta, S. K. (1997): Axisymmetric guided waves in jointed laminated cylinders, *ASCE Journal of Engineering Mechanics*, 123: 1020-1026.

Rokhlin, S. I.; Wang, W. (1992): Double through-transmission bulk wave method for ultrasonic phase velocity measurement and determination of elastic constants of composite materials, *Journal of the acoustical society of America* 91(6): 3303-3312.

Sheen, D.; Seo, S.; Cho, J. (2003): A Level Set Approach to Optimal Homogenized Coefficients , *CMES: Computer Modeling in Engineering & Sciences*, 4(1): 21-30

Sribar, R. (1994): *Solutions of inverse problems in elastic wave propagation with artificial neural networks*. Dissertation, Cornell University. 1994.

Skovoroda, A. R.; Goldstein, R. V. (2003): The Identification of Elastic Moduli of a Stratified Layer Through Localized Surface Probes, with Biomedical Applications, *CMES:Computer Modeling in Engineering & Sciences*, 4(3&4): 457-472

Takahashi, K.; Chou, T-W. (1987): Non-linear deformation and failure behavior of Carbon/Glass hybrid lam-inates, *Journal of Composite Materials* 21: 396-407.

Verbis, J. T.; Tsinopoulos, S. V.; Polyzos, D. (2002): Elastic wave propagation in fiber reinforced composite materials with non-uniform distribution of fibers, *CMES: Computer Modeling in Engineering & Sciences*, 3(6): 803-814

Vinson, J. R.; Sierakowski, R. L. (1987): *The behavior of structures composed of composite materials*, Martinus Nijhoff, Dordrecht.

Xi, Z. C.; Liu, G. R.; Lam, K. Y.; Shang, H. M. (2000): Strip element method for analyzing wave scattering by a crack in an immersed laminated composite cylinder, *The Journal for Acoustical Society of America,* 108(1): 175-183.

Yuan, F. G.; Hsieh, C. C. (1988): Three-dimensional wave propagation in composite cylindrical shell, *Composite Structures*, 42: 153-167.

Zhuang, W.; Shah, A. H.; Dong, S. B. (1999): Elasto-dynamic Green's function for laminated anisotropic circular cylinders, *Journal of Applied Mechanics*, 6: 665-674.